5. Snigirev, A., Kohn, V., Snigireva, I. & Lengeler, B. A compound refractive lens for focusing high-energy X-rays. *Nature* **384**, 49–51 (1996).
6. Schmahl, G., Rudolph, D., Guttmann, P. & Christ, O. in *Zone Plates for X-ray Microscopy* Vol. 43 *X-ray Microscopy* (eds Schmahl, G. & Rudolph, D.) 63–74 (Springer Series in Optical Sciences, Academic, London, 1984).
7. Michette, A. G. *Optical Systems for Soft X-Rays* 193–194 (Plenum, New York, 1986).
8. Spector, S. J., Jacobsen, C. J. & Tennant, D. M. Process optimization for production of sub-20 nm soft X-ray zone plates. *J. Vac. Sci. Technol. B* **15**, 2872–2876 (1997).
9. Cappellini, V., Constantinides, A. G. & Emiliani, P. *Digital Filters and their Applications* Vol. 4 *Techniques of Physics* (eds March, N. H. & Daglish, H. N.) 65–74 (Springer, Berlin, 1981).

Water conduction through the hydrophobic channel of a carbon nanotube

G. Hummer*, J. C. Rasaiah*† & J. P. Noworyta†

* *Laboratory of Chemical Physics, National Institute of Diabetes and Digestive and Kidney Diseases, National Institutes of Health, Bethesda, Maryland 20892-0520, USA*
† *Department of Chemistry, University of Maine, Orono, Maine 04469, USA*

Confinement of matter on the nanometre scale can induce phase transitions not seen in bulk systems[1]. In the case of water, so-called drying transitions occur on this scale[2–5] as a result of strong hydrogen-bonding between water molecules, which can cause the liquid to recede from nonpolar surfaces to form a vapour layer separating the bulk phase from the surface[6]. Here we report molecular dynamics simulations showing spontaneous and continuous filling of a nonpolar carbon nanotube with a one-dimensionally ordered chain of water molecules. Although the molecules forming the chain are in chemical and thermal equilibrium with the surrounding bath, we observe pulse-like transmission of water through the nanotube. These transmission bursts result from the tight hydrogen-bonding network inside the tube, which ensures that density fluctuations in the surrounding bath lead to concerted and rapid motion along the tube axis[7–9]. We also find that a minute reduction in the attraction between the tube wall and water dramatically affects pore hydration, leading to sharp, two-state transitions between empty and filled states on a nanosecond timescale. These observations suggest that carbon nanotubes, with their rigid nonpolar structures[10,11], might be exploited as unique molecular channels for water and protons, with the channel occupancy and conductivity tunable by changes in the local channel polarity and solvent conditions.

We designed a short[12] uncapped, single-walled nanotube 13.4 Å long with a diameter of 8.1 Å, and simulated for 66 ns the dynamics of this nanotube solvated in a water reservoir. Despite its strongly hydrophobic character, the initially empty central channel of the nanotube is rapidly filled by water from the surrounding reservoir, and remains occupied by about five water molecules during the entire 66 ns (Fig. 1a). These water molecules form a hydrogen-bonded chain (Fig. 1c). The number of water molecules, N, fluctuates between 2 and 7, with $N = 2$ occurring only once in 66 ns (Figs 1a and 2a). The radial and axial density profiles of the water in the nanotube show considerable structure and density depletion at the nanotube openings (Figs 2b and c).

Water molecules entering the nanotube lose on average two out of four hydrogen bonds. Only a fraction of the lost energy (~ 10 kcal mol^{-1}) can be recovered through van der Waals interactions with the carbon atoms of the nanotube (~ 4 kcal mol^{-1}), while electrostatic interactions with water molecules beyond the nanotube wall are found to be negligible. Considering this loss of hydrogen bonding, and the weak attraction of water to the nanotube carbon atoms, with a Lennard–Jones well depth of only about 0.114 kcal mol^{-1}, this persistent hydration of the nanotube interior seems surprising, but is consistent with the experimentally inferred adsorption of water onto nanotubes[13]. Further support comes from recent simulations[14] showing that a potassium iodide melt would be sucked into carbon nanotubes to form nano-crystallites, despite favourable solvation in the surrounding liquid.

The water occupancy of the channel is determined by the local excess chemical potential, $\mu_{\mathrm{nt}}^{\mathrm{ex}}$, defined as the negative free energy of removing a water molecule from the channel. This free energy is dominated not by how strongly bound a water molecule is on average, but by how populated weakly bound states are (see Methods, equation (2)). The average binding
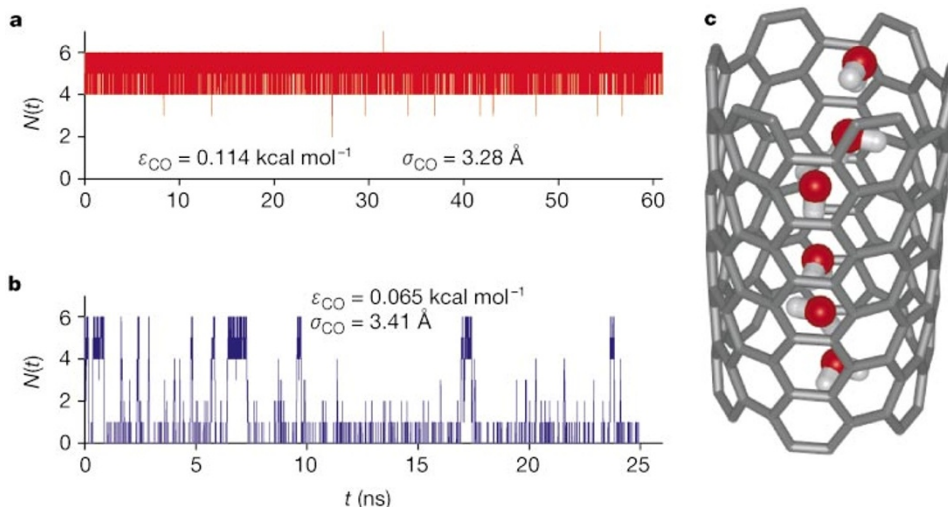

Figure 1 Water occupancy. **a, b**, Number N of water molecules inside the nanotube as a function of time for sp^2 carbon parameters (**a**) and reduced carbon–water attractions (**b**). **c**, Structure of the hydrogen-bonded water chain inside the nanotube.

energy of water molecules inside the nanotube is indeed unfavourable compared to bulk water. Nevertheless, the binding energies inside the nanotube are more sharply distributed (Fig. 3a), and high-energy states dominating the free energy are less frequently occupied. As a consequence, although water molecules at the centre of the nanotube (within 0.8 Å of the cylinder axis) lose on average 2 kcal mol^{-1} in energy, they have a lower excess chemical potential of $\mu_{nt}^{ex} \approx -6.87 \pm 0.07$ kcal mol^{-1}, compared to bulk TIP3P water ($\mu_{w}^{ex} \approx -6.05 \pm 0.02$ kcal mol^{-1}). The resulting chemical-potential difference (Fig. 3b) of $\mu_{nt}^{ex} - \mu_{w}^{ex} \approx -0.82 \pm 0.09$ kcal mol^{-1} agrees with the estimate from the average occupancy number, $-k_B T \ln(\langle N \rangle / \rho_0 \Delta V) = -0.87$ kcal mol^{-1} (see Methods, equation (1)).

Hydrogen bonds inside the nanotube are shielded from fluctuations in the environment. Only 0.02% of water pairs in contact (within 3.5 Å oxygen-atom distance) are unbound with a pair energy $u_{ij} > 0$, compared to 15% in bulk water. Hydrogen bonds in the nanotube are highly oriented, with less than 15% of the H–O···O angles exceeding 30°, compared to 37% in bulk water. The average lifetime of a hydrogen bond[15] (oxygen distance ≤ 3.5 Å, hydrogen-bond angle $\leq 30°$) is 5.6 ps, compared to 1.0 ps for bulk water. OH bonds involved in hydrogen bonds are nearly aligned with the nanotube axis, collectively flipping direction[16] every 2–3 ns on average. Despite this quasi-one-dimensional order, the water chain retains considerable entropy: water molecules can rotate freely about their aligned hydrogen bonds, resulting in a degenerate energetic 'ground state' and the narrow distribution of binding energies shown in Fig. 3a.

Water molecules not only penetrate into, but are also conducted through, the nanotube. During the 66 ns, 1,119 water molecules entered the nanotube on one side and left on the other side, corresponding to an average of about 17 water molecules per
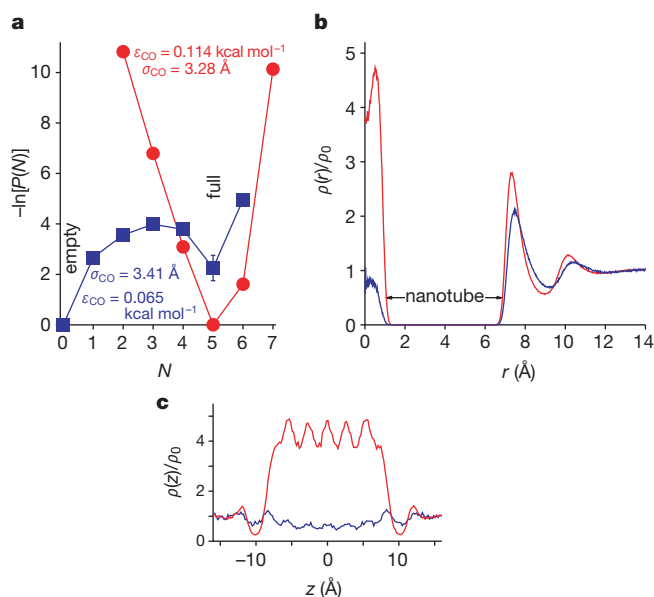

Figure 3 Water binding energies. **a**, Probability distribution $p_{bind}(u)$ of binding energies u for bulk water (blue) and water inside the nanotube (red; with a cylindrical volume of radius 0.8 Å from the nanotube axis and a height of about 13.4 Å). Vertical arrows indicate average binding energies. Tilted black arrows indicate the cross-over region, in which weakly bound states are more populated in bulk water. **b**, $\ln[p_{bind}(u)/p_{ins}(u)]$ for water inside the nanotube (filled circles) and in bulk TIP3P water (open circles), fitted to $\beta(\mu_w^{ex} - u)$ (lines). The vertical distance between the parallel lines of slope $-\beta$ gives the difference in the excess chemical potentials, $\beta(\mu_w^{ex} - \mu_{nt}^{ex})$, as indicated by green arrows.

nanosecond passing through the nanotube (51×10^{-14} cm^3 s^{-1}). The measured water flow through the twice as long channel of the transmembrane protein aquaporin-1 is of comparable magnitude[17]. Water conduction occurs in pulses through the nanotube with peaks of about 30 water molecules per nanosecond (Fig. 4a), reminiscent of single ion channel activity[18]. Slow fluctuations of the occupancy number have been observed by simulation in the pore region of a synthetic transmembrane channel[19]. The burst-like water conduction follows from the tight hydrogen-bond network inside the nanotube. Rupturing the water chain is energetically costly, and thus rare. Fluctuations outside the nanotube lead to highly concerted, yet rapid, drift-like motion of the water molecules along the nanotube axis[7–9], resulting in bursts in the water flow (Fig. 4). During those bursts, the water chain moves with little resistance through the 'greasy' nanotube, unhindered by interactions with the hydrophobic wall (Fig. 4b).

To explore the role of attractive interactions[20,21], we reduce the depth of the carbon–water van der Waals potential well by 0.05 kcal mol^{-1} (see Methods). Modifying the attractive potential mimics changes in the local polarity and solvent conditions. This seemingly small perturbation of the nanotube drastically affects its water occupancy, which fluctuates in sharp transitions between empty and filled states during a 25-ns simulation (Fig. 1b). Intermediate states are rarely populated (Fig. 2a), reflecting the large

Figure 2 Energetics and structure of nanotube water. **a**, Free energy of occupancy fluctuations, $\beta F(N) = -\ln p(N)$, where $p(N)$ is the probability of finding exactly N water molecules inside the nanotube. The approximately gaussian occupancy fluctuations[28] of the filled nanotube with sp^2 carbon parameters (red circles) become bi-modal[2] in a predominantly empty nanotube with reduced carbon–water attractions (blue squares; see Methods). **b**, Radial water density profile in units of the bulk density ρ_0, averaged over cylindrical shells centred at the axis of the nanotube, with radius r, and height determined by the carbon atoms at the nanotube rim (red, sp^2 carbon parameters; blue, modified carbon–water interactions). **c**, Water density along the nanotube axis, within a distance of 0.8 Å from the axis.
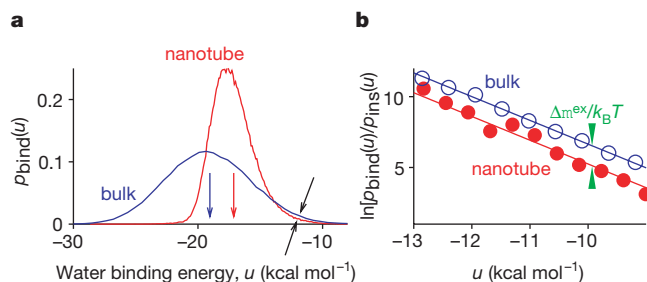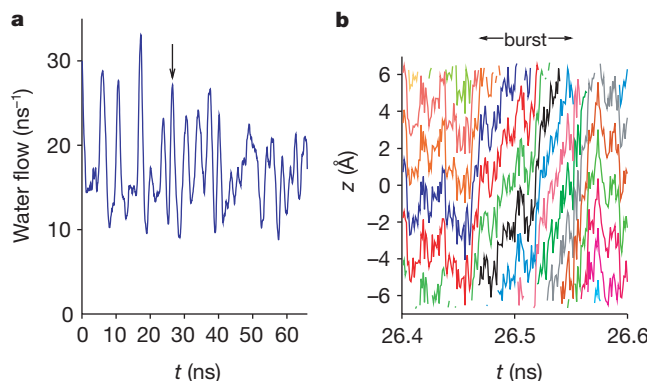

Figure 4 Flow of water through the nanotube. **a**, Number of water molecules leaving the nanotube at time t that entered the nanotube from the other side. Individual water conduction events are smoothed with a 1-ns-wide (at half-maximum) triangular filter. **b**, Motions $z(t)$ of individual water molecules shown as coloured lines, inside the nanotube along the nanotube axis during the conduction 'burst' at 26.5 ns.
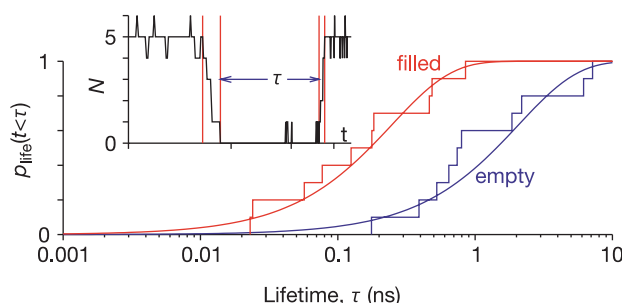
Figure 5 Kinetics of emptying and filling transitions. Cumulative distributions $P_{life}(t < \tau)$ of the lifetimes τ of the filled (red) and empty (blue) states, defined as the times between the first and last state with $N = 5$ ($N = 0$) before a transition (inset). Smooth curves are exponential distributions with the same mean.

energetic cost of fragmenting the hydrogen-bonded water chain, and leading to two-state kinetics despite the small volume. The lifetimes of the filled and empty states follow exponential distributions, with means of $\tau_{filled} = 247$ ps and $\tau_{empty} = 2,065$ ps (Fig. 5). Kinetic and equilibrium free-energy differences between filled and empty states agree, $\beta \Delta F_{kin} = \ln(\tau_{empty}/\tau_{filled}) \approx 2.1 \pm 0.5$, and $\beta \Delta F_{equil} = -\ln[\Sigma_{N=0}^{3} p(N)/\Sigma_{N>3} p(N)] \approx 2.1 \pm 0.5$ (Fig. 2a).

We conclude that, counter to intuition, hydrophobic channels can have significant water occupancy despite a reduction in the number of hydrogen bonds compared to the bulk fluid. Small changes in the nanotube–water interactions can lead to large changes in the water occupancy of the channel, with two-state transitions between empty and filled states. This might have biological significance, and offer an explanation for crystallographically empty, yet functionally filled, hydrophobic channels in proton-transferring proteins[22]. Changes in amino-acid ionization states could trigger water influx and establish protonic connectivities. Emptying/filling transitions in membrane-inserted, functionalized nanotubes, driven, for example, by light-induced excitation of covalently bound dye molecules, could potentially be used in light sensors as single-molecule 'field-effect transistors' for protonic currents. □

Methods

Molecular dynamics simulations

The 144-carbon (6,6) nanotube (13.4 Å long and 8.1 Å in diameter) is formed by folding a graphite sheet of 5×12 carbon rings to a cylinder. Solvated in a cubic box with 1,034 TIP3P water molecules[23], the nanotube is free to translate and rotate. Molecular dynamics simulations were performed at constant pressure[24] (1 bar, box length $L = 32.06 \pm 0.04$ Å) and temperature (300 K) with AMBER 6.0 (University of California at San Francisco), with particle-mesh Ewald electrostatics[25] and cubic-spline interpolation (~ 1 Å grid width). A time step of 2 fs was used. Structures were saved every 1 ps. The carbon atoms are modelled as uncharged Lennard–Jones particles with a cross-section of $\sigma_{CC} = 3.400$ Å and a depth of the potential well of $\epsilon_{CC} = 0.086$ kcal mol^{-1}, corresponding to sp^2 carbons in the AMBER96 force field[26]. Carbon–carbon bond lengths of 1.4 Å and bond angles of 120° are maintained by harmonic potentials with spring constants of 938 kcal mol^{-1} Å^{-2} and 126 kcal mol^{-1} rad^{-2}. In addition, a weak dihedral angle potential is applied to bonded carbon atoms. The carbon–water Lennard–Jones parameters are $\sigma_{CO} = 3.2751$ Å and $\epsilon_{CO} = 0.114333$ kcal mol^{-1}. We also conducted a 25-ns simulation with modified carbon–water Lennard–Jones interactions of $\sigma'_{CO} = 3.4138$ Å and $\epsilon'_{CO} = 0.06461$ kcal mol^{-1}, thus weakening the water–nanotube van der Waals attractions by a factor of about two. For reference, bulk TIP3P water was simulated for 3 ns (256 molecules, 300 K at a density of 0.987 g cm^{-3}).

Water occupancy and chemical potentials

The average number $\langle N \rangle$ of water molecules in a volume ΔV inside the nanotube is determined by the difference of the local excess chemical potential μ_{nt}^{ex} relative to that of the bulk fluid, μ_w^{ex}:

$$\langle N \rangle = \rho_0 \Delta V \exp[-\beta(\mu_{nt}^{ex} - \mu_w^{ex})] \qquad (1)$$

where $\mu_{nt}^{ex} - \mu_w^{ex}$ corresponds to a potential-of-mean-force difference for water; ρ_0 is the bulk water density; and $\beta^{-1} = k_B T$, with k_B Boltzmann's constant, and T the temperature.

Excess chemical potentials μ^{ex} are directly related to the distributions $p_{bind}(u)$ of binding energies of individual molecules:

$$\exp(\beta\mu^{ex}) = \langle \exp(\beta u) \rangle = \int p_{bind}(u) \exp(\beta u) \, du \qquad (2)$$

The binding energy u of a given water molecule is the potential-energy difference of the system in a given configuration with and without that molecule. The distribution $p_{bind}(u)$ of binding energies is related to the distribution $p_{ins}(u)$ of potential energies u of water molecules randomly inserted into the volume ΔV, and averaged over equilibrium configurations of the unperturbed system[27]:

$$\frac{p_{bind}(u)}{p_{ins}(u)} = \exp[\beta(\mu^{ex} - u)] \qquad (3)$$

Histograms for energies of water molecule removal, $p_{bind}(u)$, and insertion, $p_{ins}(u)$, were determined for bulk water, and for the central channel of the nanotube. For the nanotube histograms $p_{bind}(u)$ and $p_{ins}(u)$, water molecules were, respectively, removed from and randomly inserted into a cylindrical volume ΔV concentric with the nanotube. The radius and height of ΔV are 0.8 and 13.4 Å, as defined by the carbon atoms at the rim. Excess chemical potentials of water in the nanotube channel and in bulk TIP3P water were then determined from a histogram analysis[27] of the energy distributions by fitting $\ln[p_{bind}(u)/p_{ins}(u)]$ to $\beta(\mu_w^{ex} - u)$.

1. Gelb, L. D., Gubbins, K. E., Radhakrishnan, R. & Sliwinska-Bartkowiak, M. Phase separation in confined systems. *Rep. Prog. Phys.* **62,** 1573–1659 (1999).
2. Lum, K., Chandler, D. & Weeks, J. D. Hydrophobicity at small and large length scales. *J. Phys. Chem. B* **103,** 4570–4577 (1999).
3. Wallqvist, A. & Berne, B. J. Computer simulation of hydrophobic hydration forces on stacked plates at short range. *J. Phys. Chem.* **99,** 2893–2899 (1995).
4. Lum, K. & Luzar, A. Pathway to surface-induced phase transition of a confined fluid. *Phys. Rev. E* **56,** R6283–R6286 (1997).
5. Bolhuis, P. G. & Chandler, D. Transition path sampling of cavitation between molecular scale solvophobic surfaces. *J. Chem. Phys.* **113,** 8154–8160 (2000).
6. Stillinger, F. H. Structure in aqueous solutions of nonpolar solutes from the standpoint of scaled-particle theory. *J. Solut. Chem.* **2,** 141–158 (1973).
7. MacKay, D. H. J. & Wilson, K. R. Possible allosteric significance of water structures in proteins. *J. Biomol. Struct. Dyn.* **4,** 491–500 (1986).
8. Lynden-Bell, R. M. & Rasaiah, J. C. Mobility and solvation of ions in channels. *J. Chem. Phys.* **105,** 9266–9280 (1996).
9. Sansom, M. S. P., Shrivastava, I. H., Ranatunga, K. M. & Smith, G. R. Simulations of ion channels—watching ions and water move. *Trends Biochem. Sci.* **25,** 368–374 (2000).
10. Iijima, S. Helical microtubules of graphitic carbon. *Nature* **354,** 56–58 (1991).
11. Ajayan, P. M. & Iijima, S. Smallest carbon nanotube. *Nature* **358,** 23 (1992).
12. Liu, J. *et al.* Fullerene pipes. *Science* **280,** 1253–1256 (1998).
13. Zahab, A., Spina, L., Poncharal, P. & Marlière, C. Water-vapor effect on the electrical conductivity of a single walled carbon nanotube mat. *Phys. Rev. B* **62,** 10000–10003 (2000).
14. Wilson, M. & Madden, P. A. Growth of ionic crystals in carbon nanotubes. *J. Am. Chem. Soc.* **123,** 2101–2102 (2001).
15. Luzar, A. & Chandler, D. Hydrogen-bond kinetics in liquid water. *Nature* **379,** 55–57 (1996).
16. Pomès, R. & Roux, B. Free energy profiles for H$^+$ conduction along hydrogen-bonded chains of water molecules. *Biophys. J.* **75,** 33–40 (1998).
17. Zeidel, M. L., Ambudkar, S. V., Smith, B. L. & Agre, P. Reconstitution of functional water channels in liposomes containing purified red-cell CHIP28 protein. *Biochemistry* **31,** 7436–7440 (1992).
18. Sakmann, B., Patlak, J. & Neher, E. Single acetylcholine-activated channels show burst kinetics in presence of desensitizing concentrations of agonist. *Nature* **286,** 71–73 (1980).
19. Zhong, Q. F., Jiang, Q., Moore, P. B., Newns, D. M. & Klein, M. L. Molecular dynamics simulation of a synthetic ion channel. *Biophys. J.* **74,** 3–10 (1998).
20. Walqvist, A., Gallicchio, E. & Levy, R. M. A model for studying drying at hydrophobic interfaces: Structural and thermodynamic properties. *J. Phys. Chem. B* **105,** 6745–6753 (2001).
21. Beckstein, O., Biggin, P. C. & Sansom, M. S. P. A hydrophobic gating mechanism for nanopores. *J. Phys. Chem. B* (in the press).
22. Wikström, M. Proton translocation by bacteriorhodopsin and heme-copper oxidases. *Curr. Opin. Struct. Biol.* **8,** 480–488 (1998).
23. Jorgensen, W. L., Chandrasekhar, J., Madura, J. D., Impey, R. W. & Klein, M. L. Comparison of simple potential functions for simulating liquid water. *J. Chem. Phys.* **79,** 926–935 (1983).
24. Berendsen, H. J. C., Postma, J. P. M., van Gunsteren, W. F., Nola, A. D. & Haak, J. R. Molecular dynamics with coupling to an external bath. *J. Chem. Phys.* **81,** 3684–3690 (1984).
25. Darden, T., York, D. & Pedersen, L. Particle mesh Ewald: An N·log(N) method for Ewald sums in large systems. *J. Chem. Phys.* **98,** 10089–10092 (1993).
26. Cornell, W. D. *et al.* A second generation force field for the simulation of proteins, nucleic acids, and organic molecules. *J. Am. Chem. Soc.* **117,** 5179–5197 (1995).
27. Bennett, C. H. Efficient estimation of free energy differences from Monte Carlo data. *J. Comput. Phys.* **22,** 245–268 (1976).
28. Hummer, G., Garde, S., García, A. E., Pohorille, A. & Pratt, L. R. An information theory model of hydrophobic interactions. *Proc. Natl Acad. Sci. USA* **93,** 8951–8955 (1996).